

# Nonlinear Subsidence Rate Estimation Using Permanent Scatterers in Differential SAR Interferometry

Alessandro Ferretti, Claudio Prati, and Fabio Rocca

**Abstract**—Discrete and temporarily stable natural reflectors or permanent scatterers (PS) can be identified from long temporal series of interferometric SAR images even with baselines larger than the so-called critical baseline. This subset of image pixels can be exploited successfully for high accuracy differential measurements. We discuss the use of PS in urban areas, like Pomona, CA, showing subsidence and absidence effects. A new approach to the estimation of the atmospheric phase contributions, and the local displacement field is proposed based on simple statistical assumptions. New solutions are presented in order to cope with nonlinear motion of the targets.

**Index Terms**—Atmospheric measurements, digital elevation model (DEM) reconstruction, geodetic measurements, interferometry, phase unwrapping, radar data filtering, synthetic aperture radar (SAR).

## I. INTRODUCTION

THE MAIN goal of this paper is to present an extension of the permanent scatterers (PS) technique recently introduced in a paper submitted for publication [1]. In that paper, it is shown that scatterers exist that are coherent over several years. They can be identified from a series of ERS SAR images. A time and space analysis is then carried out to separate and identify the different contributions to the interferometric phase of each PS. Thus, relative elevation, motion, and travel path variation due to the atmosphere are jointly found, and the ground motion can be carefully measured.

The main steps of the technique can be summarized as follows [1], [2].

- 1) *Interferogram formation*: Given  $N+1$  SAR images (all the available ERS-1 and ERS-2 images on the same track),  $N$  full-resolution interferograms are formed with respect to the same master image.
- 2) *Digital Elevation Model and differential interferograms formation*: A reference digital elevation model (DEM) (in most cases it can be generated using the available ERS tandem pairs) and precise orbital data are used to get  $N$  differential interferograms.
- 3) *Preliminary estimate of LOS motion, elevation error, and atmospheric contribution*: Due to the limited accuracy of the DEM (dependent on the number and the quality of the

tandem acquisitions [3]), the local topography cannot be considered as perfectly removed, especially in high baseline interferograms. In fact, residual topographic phase contributions will be proportional to the normal baseline and the elevation error. Moreover, the motion of the target projected on the line of sight (LOS) will turn into a phase curve as a function of time. A constant velocity model is adopted for target motion. The atmospheric phase screen [1], [5]–[7], [9] (APS, i.e. atmospheric phase components) and possible phase contributions due to baseline errors are approximated (for each differential interferogram) as a linear phase term both in range and in azimuth direction. Provided that the SNR is high enough, elevation errors, LOS motion of each target (with respect to a reference pixel of known motion), and APSs parameters can be jointly estimated minimizing the temporal phase residuals. At this stage, only those pixels that are coherent enough are considered.

- 4) *Refinement of step 3*: The APS estimate is improved by spatial smoothing of the phase residues. The joint estimation of target elevation and LOS velocity is carried out again. This final step allows one to identify more PSs.

Although the results obtained with this technique were remarkable, two main limitations were noticed. Only small areas (less than  $5 \times 5$  km large) could be processed. Considering larger areas, too many parameters should be estimated and the planar approximation of the APS becomes less accurate. This may prevent the algorithm from converging. Moreover, the algorithm does not cope with nonlinear target motion: coherent scatterers undergoing a complex motion (i.e., the constant velocity model is not valid) are not identified as PSs or, in other cases, the nonlinear term of their motion is considered as part of the atmospheric contribution. This is indeed a more subtle point that needed to be addressed. As it has been noted by R. Bamler and M. VanDerKooij [8] in their independent private communications, if the phase residues are spatially low-pass interpolated (see point 4, mentioned previously) the low wavenumber components of the motion that do not match the linear model are lost, since they are merged with the APS. The low phase dispersion with respect to the constant velocity model after APS removal can then be misleading.

The problem is then to find a more general approach that can cope with nonlinear motions without introducing too many parameters. To this end, it is necessary to move from a deterministic model for PS motion to a stochastic one. The basic idea is to separate the different phase contributions (motion, APS,

Manuscript received September 6, 1999; revised March 23, 2000. This work was supported in part by an ESA-ESRIN under Contract 13557/99/I-DC.

The authors are with the Dipartimento di Elettronica ed Informazione del Politecnico, 20133 Milano, Italy (e-mail: aferre@elet.polimi.it).

Publisher Item Identifier S 0196-2892(00)08922-1.

decorrelation noise) by means of a least mean square (LMS) estimation, i.e. a Wiener filter, taking into account the spatio-temporal data distribution and the correlations between the samples. The target is to *exploit* the spatio-temporal correlation of the APSs (i.e., the atmospheric effects should be uncorrelated in time and spatially smooth). Then, a spatio-temporal model of the displacement field should be exploited. This will be subject of further studies. Models like those proposed in [20] will be useful. Here, we present a suboptimal spatio-temporal filter for motion estimation that can be adopted when no *a priori* information is available. The filter should be applied to the unwrapped phase values of the PS.

## II. UNWRAPPING ON A SPARSE GRID

Phase unwrapping of a single differential interferogram (we always refer to the ERS case) with a normal baseline of, say, 1000 m and a temporal baseline of three years even on a sparse grid of stable scatterers is impossible without *a priori* information. The task becomes feasible only in a multi-interferogram framework, where all phase data relative to the same target are jointly analyzed. Multibaseline phase unwrapping techniques have been already applied successfully for DEM reconstruction [4]. For the problem at hand, where both elevation and motion of the scatterer are to be determined, a more complex approach will be necessary. Moreover, since the APS is a low wavenumber disturbance [6], [7], it can be estimated starting from a sparse grid of points [1], [5], previously selected based on their coherence.

Phase unwrapping of irregularly sampled data has lately gained increasing attention [10], [12], although the proposed techniques have been applied to single differential interferograms characterized by low normal baseline values. As well known, phase unwrapping can be performed following a two-steps algorithm [13]

- 1) estimation of the unwrapped phase differences between neighboring pixels;
- 2) integration of the gradient using one of the known techniques (minimum cost flow [11], weighted least mean squares [13], [14], branch and cut [15]).

As far as the integration step is concerned, we used a WLMS algorithm, but other techniques can be applied as well. The key point here is the reliability of the data vector, i.e., the estimation of the phase gradient. To this end, the availability of many differential interferograms of the same area can strongly reduce the need of *a priori* information (e.g., a model for the phase [10]). Differential phase data are the sum of four contributions

$$\phi(\mathbf{x}, t_i) = \varepsilon_{topo}(\mathbf{x}, t_i) + \mu(\mathbf{x}, t_i) + \alpha(\mathbf{x}, t_i) + n(\mathbf{x}, t_i) \quad i = 1 \dots N \quad (2.1)$$

where

- $\mathbf{x}$  2-D vector specifying the position of the pixel in the image;
- $t$  time variable (more precisely  $t_i$  is the temporal baseline of the  $i$ th interferogram);
- $\varepsilon_{topo}$  phase contribution due to DEM errors;
- $\mu$  phase contribution due to a possible motion of the target in the direction of the LOS;
- $\alpha$  APS;

TABLE I  
POMONA ERS DATA SET. TRACK 170,  
FRAME 2925.  $b$  IS THE NORMAL BASELINE VALUE WITH RESPECT TO THE  
MASTER ORBIT, WHILE  $t$  IS THE TEMPORAL BASELINE

SAT	Date	$b$ [m]	$t$ [day]	#
1	19920617	-42	-1389	1
1	19920826	227	-1319	2
1	19920930	471	-1284	3
1	19930113	136	-1179	4
1	19930428	828	-1074	5
1	19930707	-973	-1004	6
1	19930915	669	-934	7
1	19931020	731	-899	8
1	19950421	-63	-351	9
1	19950526	-39	-316	10
1	19950804	383	-246	11
1	19950908	-1000	-211	12
1	19951013	851	-176	13
2	19951014	1229	-175	14
1	19951117	-567	-141	15
2	19951118	-1079	-140	16
1	19951222	698	-106	17
2	19951223	433	-105	18
1	19960126	194	-71	19
2	19960127	350	-70	20
1	19960405	89	-1	21
2	19960406	0	0	22
1	19960510	668	34	23
2	19960511	505	35	24
2	19960615	-402	70	25
2	19960824	-710	140	26
2	19960928	-154	175	27
2	19961207	-573	245	28
2	19970111	66	280	29
2	19970705	-226	455	30
2	19970809	75	490	31
2	19970913	62	525	32
2	19971018	149	560	33
2	19971122	395	595	34
2	19971227	142	630	35
2	19980131	-40	665	36
2	19980307	-554	700	37
2	19980411	-235	735	38
2	19980620	555	805	39
2	19980725	-159	840	40
2	19990116	41	1015	41

$n$  decorrelation noise.

For simplicity sake, systematic phase components due to orbit indeterminations are considered as part of the APS contribution [1]. However, their impact on the differential interferograms can be strongly reduced, for ERS satellites, using precise state vectors [23].

It is now useful to separate  $\mu(\mathbf{x}, t_i)$  into two terms

$$\mu(\lambda, t_i) = \frac{4\pi}{x} v(x) \cdot t_i + \mu_{NL}(\mathbf{x}, t_i) \quad (2.2)$$

where

- $v(\mathbf{x})$  mean velocity of target  $\mathbf{x}$ ;
- $\lambda$  system wavelength (5.66 cm for ERS);
- $\mu_{NL}$  residual (nonlinear) motion.

If we denote by  $b_i$  the normal baseline of the  $i$ th interferogram, we can finally write

$$\phi(\mathbf{x}, t_i) = C_{\varepsilon}(\mathbf{x}) \cdot b_i + C_v(\mathbf{x}) \cdot t_i + w(\mathbf{x}, t_i) \quad (2.3)$$



Fig. 1. Pomona, CA: multi-image reflectivity map in SAR coordinates. The test site is about  $16 \times 20$  km wide.

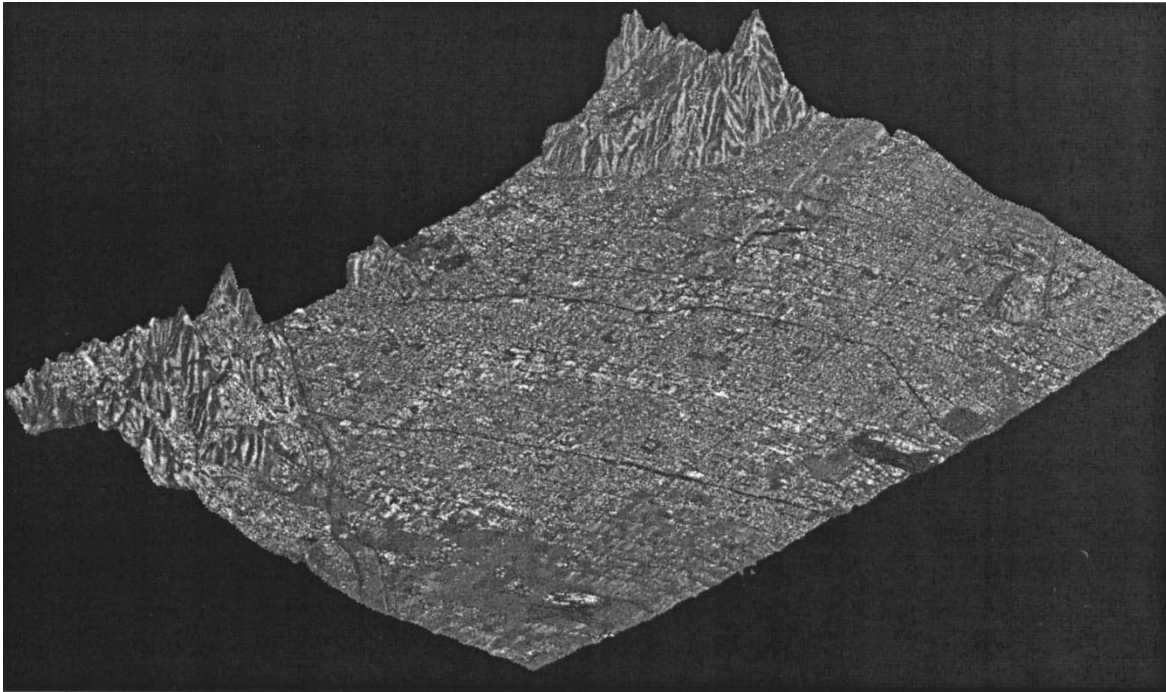


Fig. 2. Three-dimensional (3-D) perspective view of the test site. Data have been resampled in UTM coordinates. The DEM has been estimated using four tandem pairs. Estimated accuracy:  $\sim 10$  m.

where

$C_{\varepsilon}$  proportional to the elevation error in  $\mathbf{x}$ ;

$C_v$  proportional to the mean velocity of the target;

$w(\mathbf{x}, t_i)$  (to be called linear phase residues; LPR) is the sum of the three contributions: APS, noise, and non-linear motion.

For phase unwrapping, we have to estimate the phase *difference*

between two neighboring pixels

$$\begin{aligned} \Delta\phi(\mathbf{x}_r, \mathbf{x}_s, t_i) &= \phi(\mathbf{x}_r, t_i) - \phi(\mathbf{x}_s, t_i) \\ &= \Delta C_{\varepsilon} \cdot b_i + \Delta C_v \cdot t_i + \Delta w_i \end{aligned} \quad (2.4)$$

where  $\Delta C_{\varepsilon}$  and  $\Delta C_v$  will be proportional to the residual elevation difference  $\Delta z$  and the mean velocity difference  $\Delta v$  between

$\mathbf{x}_r$  and  $\mathbf{x}_s$ , respectively. It should be noted that if we knew  $\Delta z$  and  $\Delta v$  and the condition

$$|\Delta w_i| < \pi \quad (2.5)$$

is satisfied, we can easily unwrap  $\Delta\phi(\mathbf{x}_r, \mathbf{x}_s, t_i)$ . An estimation of both  $\Delta z$  and  $\Delta v$  directly from the  $N$  wrapped interferograms available is indeed possible. In fact, the problem is to find the bidimensional frequency of a complex sinusoid

$$e^{j\Delta\phi(\mathbf{x}_r, \mathbf{x}_s, t_i)} = e^{j(\Delta C_{\epsilon} \cdot b_i + \Delta C_v \cdot t_i + \Delta w_i)} \quad (2.6)$$

( $j = \sqrt{-1}$ ) sampled on an irregular grid  $\{b_i, t_i\}$ . This can be accomplished using one of the well known techniques developed in spectral analysis, though data are usually considered uniformly sampled [16]. For the problem at hand, we used a simple periodogram. Some observations are now in order.

- 1) Condition (2.5) implies that the phase dispersion with respect to the linear model be low. On the other hand, the root mean square (rms) values of the phase residues after local phase detrending using the periodogram will be a function of  $\sigma_{\Delta w}$ , too. Therefore, the local value of the multi-image phase coherence

$$\gamma \triangleq \left| \frac{\sum_{i=1}^N e^{j\Delta w_i}}{N} \right| \quad (2.7)$$

can be adopted as a reliability measure for each equation used for phase unwrapping. In our implementation, pairs with  $\gamma < \gamma_0$  are discarded, while the others are  $\gamma$ -weighted.

- 2) Since  $\Delta\mu_{NL}$ ,  $\Delta\alpha$ , and  $\Delta n$  are independent random variables, the residual phase variance  $\sigma_{\Delta w}^2$  is the sum of three contributions

$$\sigma_{\Delta w}^2 = \sigma_{\Delta\mu_{NL}}^2 + \sigma_{\Delta\alpha}^2 + \sigma_{\Delta n}^2. \quad (2.8)$$

Nevertheless, low  $\sigma_{\Delta w}$  values are usually obtained for most of the pixel pairs. First,  $\mathbf{x}_r$  and  $\mathbf{x}_s$  were previously selected as locations of highly coherent targets, and they should be only slightly affected by decorrelation noise (low  $\sigma_n^2$ ). Then,  $\mathbf{x}_r$  and  $\mathbf{x}_s$  are close by pixels. This implies low variance of the atmospheric component  $\Delta\alpha$ . For points less than 1 km apart, values of  $\sigma_{\Delta\alpha}^2$  less than 0.1 rad<sup>2</sup> are common [5]. Finally, the motion of neighboring pixels is usually correlated (see the following section). If this hypothesis is verified,  $\sigma_{\Delta\mu_{NL}}^2$  should be low as well. On the contrary, if the motion of the targets in the area of interest is highly nonlinear and spatially uncorrelated, a higher density of PS (lower  $\sigma_{\Delta\alpha}^2$ ) is necessary and possibly a higher coherence level of the scatterers (lower  $\sigma_{\Delta n}^2$ ).

- 3) If the PS density is very low, there could be large gaps where no PS can be identified. If the area of interest is fragmented into several clusters of PS and no reliable equation is available between them ( $\gamma < \gamma_0$ ), the proposed methodology should be applied to each cluster and *a priori* information (e.g., a model of the displacement field or GPS measurements) should be used to carry out the ‘‘patching’’ of the clusters.

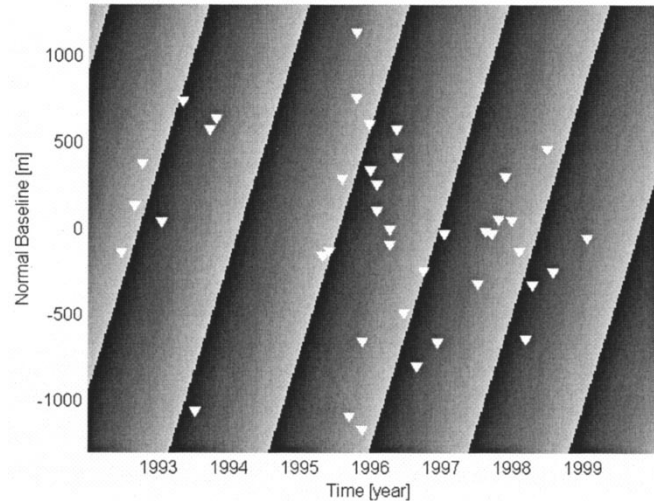


Fig. 3. Space-time distribution of the available data. The bidimensional complex sinusoid represent the phase contribution for a LOS velocity of 2 cm/yr and a DEM error of 5 m (see text).

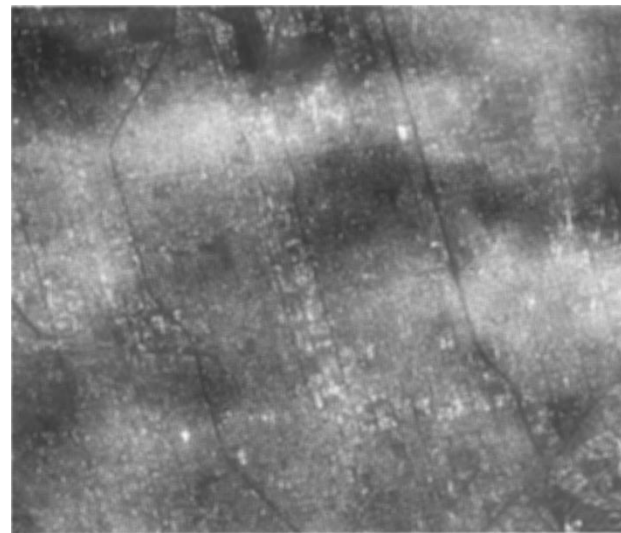


Fig. 4. Example of the atmospheric phase screen (APS) estimated for April 6, 1996 (master image of the data set). The atmospheric phase contribution has been superimposed on the multi-image reflectivity map of the area. APS standard deviation is 0.86 rad.

- 4) High values of  $\gamma$  imply a good estimation of  $\Delta z$  and  $\Delta v$ , so by integrating  $\Delta z$ , it is possible to refine the DEM on the PS set, starting from a PS of known elevation and motion. As far as the displacement field is concerned, though the mean velocity of the targets can be obtained integrating the values  $\Delta v$ , a more precise estimation should take into account the nonlinear term of the motion, as will be presented in the following section.

We can summarize the results of this section as follows. Phase unwrapping of differential interferograms characterized by high geometrical and temporal baseline is usually possible only on a sparse grid of PS and using a multi-image approach. The mathematical framework is easier if the constant velocity model can be applied. This hypothesis is not a real constraint and the technique can cope with nonlinear target motion, provided that the PS density and coherence is high enough. Phase differences are

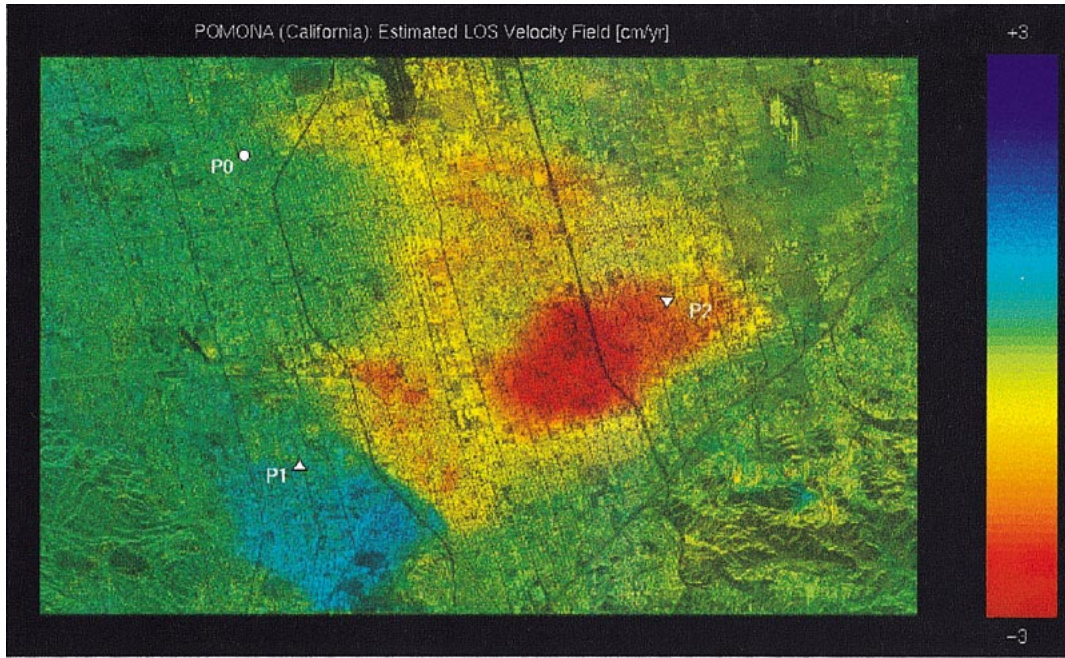


Fig. 5. Pomona: estimated mean velocity field (in the direction of the line of sight) in cm/yr. Point  $P_0$  corresponds to the reference pixel (supposedly stable and of known elevation), while  $P_1$  and  $P_2$  show the locations of the PSs analyzed in Figs. 6 and 7.

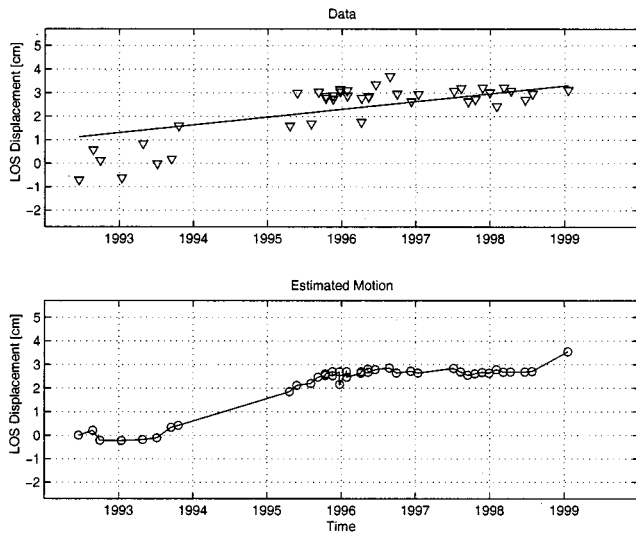


Fig. 6. An example of a time series relative to one of the PSs identified in the inflating area (point  $P_1$  in Fig. 5). On the top of the picture, data compensated only for the estimated DEM error are reported together with the estimated linear component of the motion. The estimated motion after APS removal reveals a noticeable departure from the constant velocity model.

unwrapped taking advantage of the estimated values of relative velocity  $\Delta v$  and relative elevation  $\Delta z$  of each scatterers pair. Phase data are then integrated using one of the techniques used for unwrapping of regularly samples data and local values of  $\gamma$  can be used as data weights. Finally, integration of  $\Delta z$  values allows one to refine the reference DEM on the PS set.

### III. SPACE-TIME ESTIMATION

Once phase data are unwrapped, it is possible to estimate the signal component of interest  $s(\mathbf{x}, t)$  (e.g.,  $\alpha(\mathbf{x}, t)$  or  $\mu(\mathbf{x}, t)$ ) by properly weighting the data vector  $\phi$ . As is well known, the

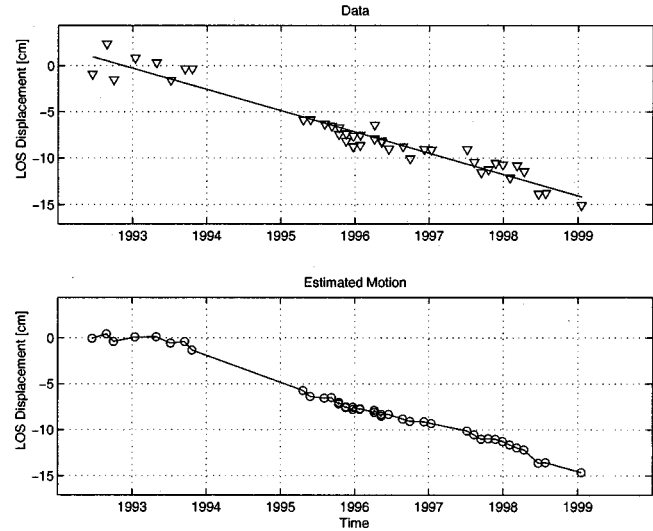


Fig. 7. An example of a time series relative to one of the PSs identified in the subsiding area (point  $P_2$  in Fig. 5). On the top of the picture, data compensated only for the estimated DEM error are reported together with the estimated linear component of the motion. The estimated motion after APS removal reveals a noticeable departure from the constant velocity model.

weights are solutions of the following system of equations [18], [19]:

$$\mathbf{R}_{\phi\phi} \cdot \mathbf{f}(\mathbf{x}, t) = \mathbf{r}_{\phi s}(\mathbf{x}, t) \quad (3.1)$$

where  $\mathbf{R}_{\phi\phi} = E[\phi \cdot \phi^T]$  is the data correlation matrix, and  $\mathbf{r}_{\phi s} = E[\phi \cdots (\mathbf{x}, t)]$  is the crosscorrelation vector between the data and the signal under estimation. It should be noted that the optimum filter  $\mathbf{f}$  is space and time variant. In fact, since we deal with a sparse spatio-temporal distribution of samples,  $\mathbf{r}$  is a function of  $(\mathbf{x}, t)$ . On the contrary,  $\mathbf{R}_{\phi\phi}$  is fixed once the spatio-temporal data distribution is known. The key point

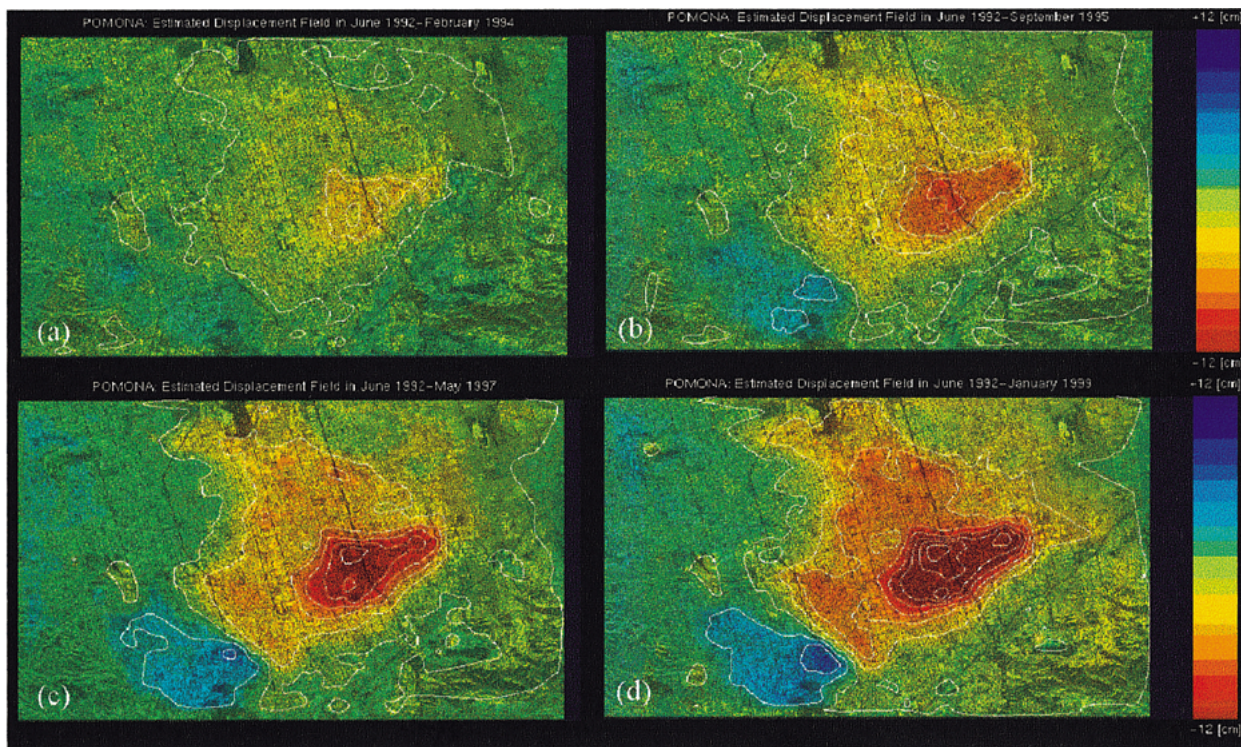


Fig. 8. Estimated displacement field (in the direction of the line of sight) in Pomona. Four snapshots corresponding to four different time intervals (the sampling interval is about 560 days) are reported: (a) June 1992–February 1994; (b) June 1992–September 1995; (c) June 1992–May 1997; (d) June 1992–January 1999.

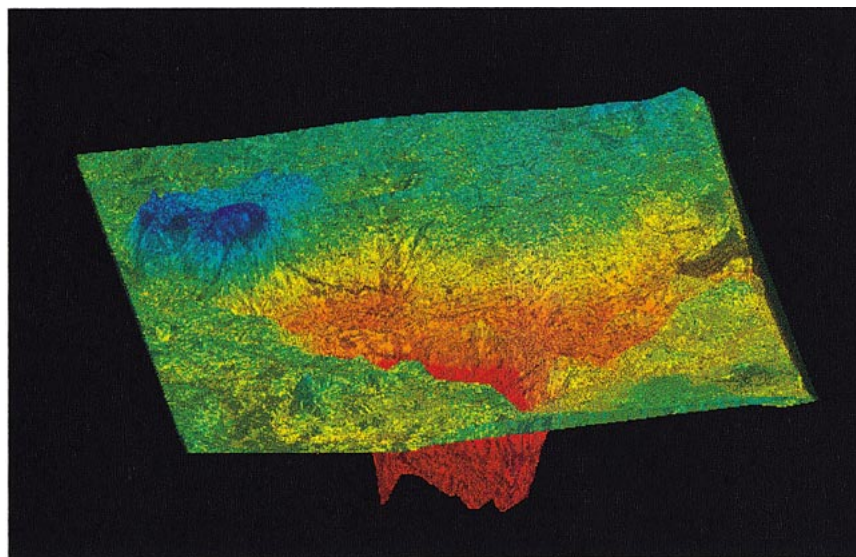


Fig. 9. Perspective view of the displacement field (in the direction of the line of sight) relative to June 1992–January 1999. Minimum negative value:  $-20$  cm. Maximum positive displacement:  $+6$  cm.

TABLE II  
COMPARISON BETWEEN THE PS TECHNIQUE AND CONVENTIONAL DIFFERENTIAL SAR INTERFEROMETRY (DInSAR)

	PS Technique	Conventional DInSAR
1 Baseline	no limits in the ERS database	very small ( $< 200$ meters)
2 Atmospheric Artifacts	strongly reduced	no reduction
3 Coherence	$> 0.7$ on a single pixel	$> 0.3$ on several adjacent pixels
4 DEM accuracy	100 meters	baseline dependent
5 # of SAR images	$> 30$	$\geq 2$

for optimum filtering is the estimation of the correlation values. While an expression of the correlation matrix of the atmospheric

component can be obtained from Kolmogorov theory [5], a statistical description of the local displacement field can be a very difficult task to achieve.

Basically, this choice should reflect our knowledge of the physical phenomenon we are dealing with (an example of mathematical modeling of a subsiding area is given in [20]). If a model is available, parameters and expressions of the correlation matrix assume a specific physical meaning (see [21] and references therein). In general, the lack of a physical model does not allow an accurate estimation of the correlations and so the optimum filter can not be implemented.

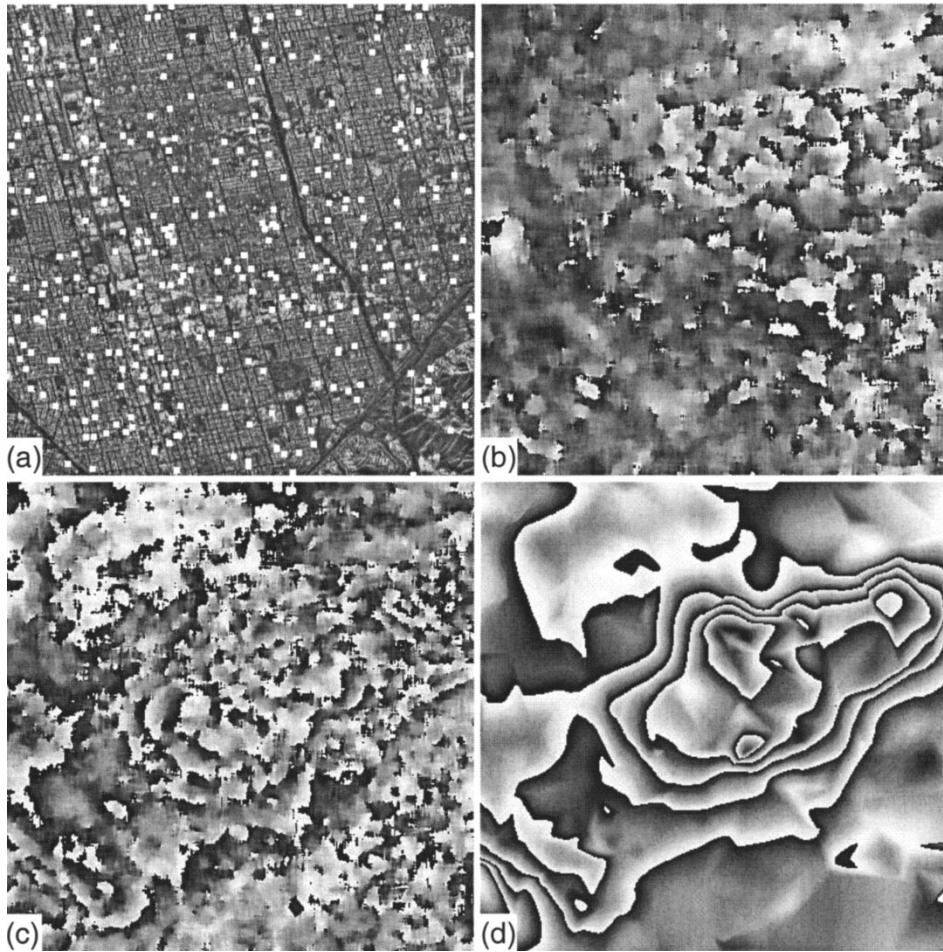


Fig. 10. Comparison with conventional DInSAR technique: location of the PSs identified in the subsiding area. (a) Differential interferogram 19930 113–19971 227:  $b = 6$  m,  $t = 1809$  day. (b) Difference between (d) and (c). (c) Pseudo-interferogram obtained interpolating the terrain deformation measured in correspondence of the PSs (no smoothing has been performed) (d). Difference between (d) and (c); data have been low-pass filtered for visualization purposes.

Besides, the computational burden of this estimation technique is huge due to the very large number of data involved. Inversion of matrix  $\mathbf{R}_{\phi\phi}$  may be impractical even considering only a small neighborhood around the point under estimation. If no *a priori* information is available about the displacement field of the area of interest, a possible approach that can be adopted is the whitening of the time series of the LPR samples  $w(\mathbf{x}, t_i)$ . Once the residual phases of the PSs have been obtained (data detrended for the estimated DEM errors and the mean velocity field), we can start looking at their temporal evolution, to check for subsidence leakage. The mean value  $\bar{w}(\mathbf{x})$  of the residual phases is an estimation of the atmospheric phase contribution of the master image in  $\mathbf{x}$  (common to all the differential interferograms), while the low pass component of  $[w(\mathbf{x}, t_i) - \bar{w}(\mathbf{x})]$  should be considered as an estimation of the nonlinear motion contribution  $\mu_{NL}(\mathbf{x}, t_i)$ . APS estimation is then carried out by smoothing spatially the high-pass filtered LPR time series

$$\hat{\alpha}(\mathbf{x}, t_i) = [[w(\mathbf{x}, t)]_{HP\_Time}]_{LP\_Space} + [\bar{w}(\mathbf{x})]_{LP\_Space} \quad (3.2)$$

with obvious symbol meaning. The first term in (3.2) is then an estimation of the atmospheric phase contribution superimposed on the single SAR image acquired at time  $t_i$ . The fil-

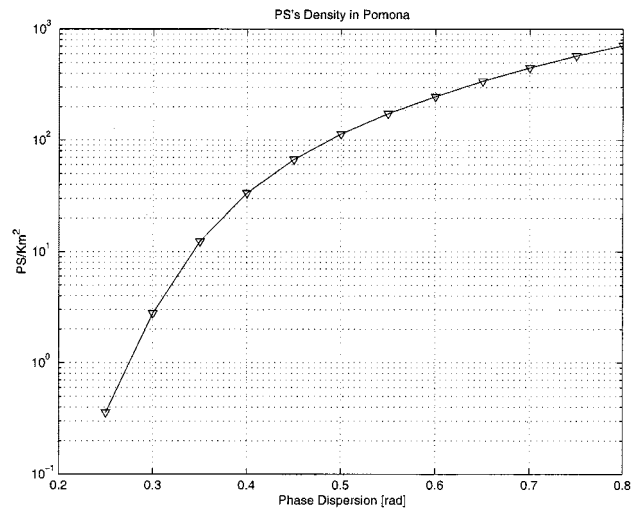


Fig. 11. PS density (cumulative) per square kilometer as a function of the maximum phase dispersion allowed (with respect to the linear model).

tered atmospheric component relative to the master acquisition is then added back to get the APS of each differential interferogram. To make it simple, we can carry out for each pixel a temporal smoothing using a triangular filter and remove the low

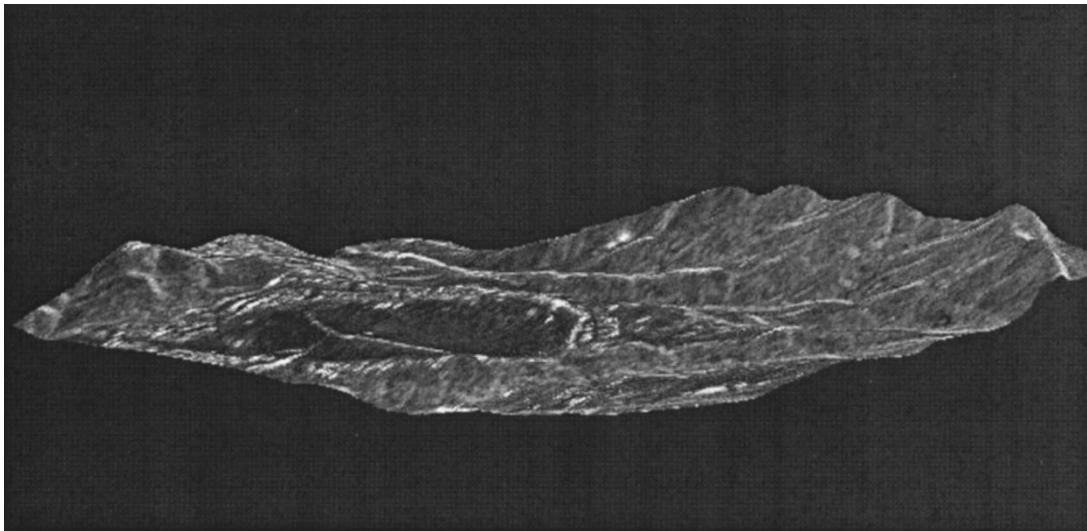


Fig. 12. Perspective view of the reference DEM of a small area near Pomona. For visualization purposes, the vertical axis has been magnified (maximum relative elevation difference is  $\sim 50$  m).

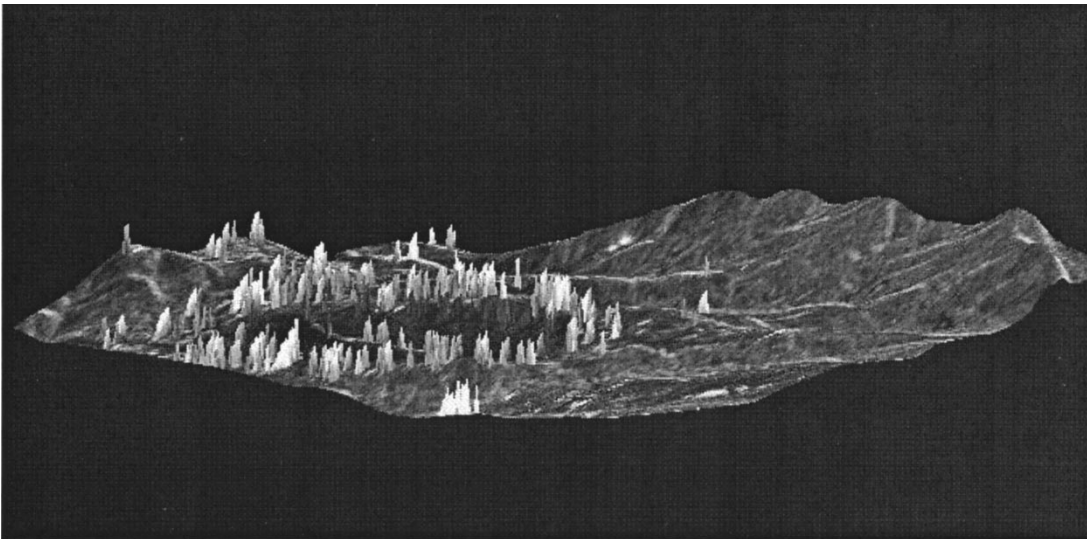


Fig. 13. Perspective view of the DEM optimized in correspondence of the PSs identified in the area shown in Fig. 12.

pass component. Phase residuals are then spatially filtered using a moving average on a  $2 \times 2$  km window. As described in [1], after estimation and removal of all the APS superimposed on the data, we can finally estimate the motion of each pixel in the image and identify more PSs.

#### IV. A STUDY OF SUBSIDENCE IN POMONA (CA)

##### A. The Available Data

An interesting case of subsidence, already studied using differential interferometry and other techniques, is found in Pomona [22]. The data set used is presented in Table I. 41 ERS images were available. All were resampled on the same master acquisition (ERS2: April 6th, 1996) and 40 interferograms were obtained. In Fig. 1 the incoherent average of all the data (multi-image reflectivity map) is reported. Due to the high number of looks, the radiometric quality of this image is comparable to that of an optical one. The area is

about  $16 \times 20$  km wide. Using four tandem pairs, we also determined a reference DEM (about 10 m accuracy, also limited by building effects) of the area of interest using the technique of [3], [4] (Fig. 2), and the corresponding phase was removed from each single image using DEOS precise state vectors [23].

##### B. Selection of PS Candidates and APS Removal

After the initial selection of the PS set (about 3 PS/km<sup>2</sup> were identified), phase increments between each PS and all the others less than 1 km apart were estimated using the periodogram technique. To better illustrate this kind of approach, in Fig. 3 we show the temporal distribution of the takes together with their normal baselines, referred to the master image. The range of normal baselines is about  $\pm 1100$  m, while the maximum temporal baseline is more than six years. If a PS had an LOS velocity of, say, 2 cm/yr and a residual elevation difference of 5 m with respect to a neighboring scatterer, considered as a reference, its phase variations as a function of time and baseline would be a

2-D phase ramp, also represented in the Fig. 3. If now we accept, temporarily, the hypothesis of constant LOS velocity of each pixel, then using a simple periodogram (albeit with an irregular sampling of the two dimensions: baselines and time), we could estimate both the residual elevation and the LOS velocity difference of the pixels. Analysis of Fig. 3 also tells us that the precision of the estimate of the vertical elevation is a good indicator of the quality of the estimate of LOS velocity in that there is no particular reason why the estimation should be any better in one rather than in the other dimension. As already mentioned, this operation was carried out for PS pairs with  $\gamma > 0.75$  [see definition (2.7)] and less than 1 km apart, thus removing the effects of the residual elevation with respect to the average DEM and of the LOS velocity and estimating the unwrapped phase values.

After phase unwrapping, time series analysis of the LPR values of each PS was carried out. The target is to identify possible nonlinear motion contributions. As discussed in Section III, if we could model the spatial and the temporal behavior of the phenomenon, we could implement an optimum LMS filter. For the problem at hand, since we lacked a physical model of the phenomenon, we used the approach outlined in Section III. For each PS, we carried out a temporal smoothing of the LPRs using a triangular filter (300 days long), and we removed the low pass component. Phase residuals were then spatially filtered using a moving average on a  $2 \times 2$  km window (3.2). APSs were then interpolated on the original regular grid and removed from each datum. An example of estimated APS (relative to the master acquisition) is reported in Fig. 4. Rms values of the 41 estimated APSs range from 0.25–1.35 rad.

### C. Displacement Field Estimation

After APS removal, we can finally estimate the motion of each pixel in the image and identify more PSs. Both DEM errors and target motion can now be estimated on a PS-by-PS basis. The mean LOS velocity field is reported in Fig. 5. In this picture, not only the subsidence but an inflating area is clearly visible (with respect to the reference point  $P_0$  shown in Fig. 5). In fact, an abrupt change in the velocity sign can be noted in the lower part of the image. The mean velocity field is only a first order approximation of the local displacement vector, though most of the energy (more than 90%) of the motion phase contribution  $\mu$  in the test site is given by the linear term. Nevertheless, severe departures from a uniform motion were detected near the inflating area and where high subsidence velocity values ( $> 2$  cm/yr) were measured. Two examples are shown in Figs. 6 and 7. Unfortunately, no ground truth data were available.

Of course, after APS removal it is possible to estimate not only the mean LOS velocity field of the area but a displacement field as a function of time, possibly interpolating the displacement maps on a regular temporal grid. The display of the outcomes of the results is an issue of considerable importance [21]. Here, we report a sequence of four spatial maps corresponding to four time instants between June 1992 and January 1999 (Fig. 8). The nonlinear motion behavior reflects into the change of shape of the contour lines. A perspective view of the displacement field of Fig. 8(d) is also depicted in Fig. 9, where

the different amplitude of the displacement of the uplifting and the subsiding areas can be better appreciated. Maximum positive and negative displacements are +6 and -20 cm, respectively. Of course, computer animation procedures can provide an improved visualization of the phenomenon under study. Two animations relative to the estimated displacement field in Pomona since June 1992 are available on our web site [26].

### D. Comparison with Conventional Differential Interferometry

It is well known that some coherence can often be found on urban areas even after long time interval [25]. PSs are usually found in urban areas, too. The reader could then be interested in comparing the results that can be obtained by means of the PS and the “usual” differential SAR interferometry (DInSAR) techniques. In Table II, we tried to summarize advantages and drawbacks of both techniques. Some observations are in order.

- 1) Using the PS technique, all the available SAR images recorded by ERS-1 and ERS-2 can be exploited without concern for the baseline. On the contrary, only small baselines should be selected for differential interferometry with a consequent loss of time coverage.
- 2) Atmospheric artifacts with low spatial frequency can be practically eliminated. It is a serious limitation of differential interferometry whenever the terrain deformation is small and spatially smooth.
- 3) Single coherent pixels can be identified. This feature is essential in the case of large temporal and geometric baselines, when only pointwise targets carry useful phase information.
- 4) A coarse DEM can be used in the PS technique since the accurate elevation of each PS is computed. A better DEM would only reduce the computational time. This is not the case for differential interferometry where the required DEM accuracy is inversely proportional to the normal baseline of the images used for motion detection.
- 5) In our opinion, the advantages offered by the PS technique widely justify the need of a large number of images.

A visual comparison of the results achievable on Pomona with the two techniques is shown in Fig. 10. A few images among the available data set allow to generate usable interferograms. One of the most favorable pairs (the baseline is 6 m) has been selected. The time interval between the two takes is about five years. The complex interferogram has then been filtered in order to reduce the noise, and the resulting fringes are shown in Fig. 10(c). For the sake of comparison, the terrain deformation measured by means of the PS technique [interpolated from the PS measures shown in Fig. 10(a)] has been wrapped at 2.8 cm, thus generating the pseudo-interferogram reported in Fig. 10(d). The difference between the two interferograms is then shown in Fig. 10(b).

It should be noted that even in the most favorable case for differential interferometry (i.e., very low normal baseline values), the quality of the result is dramatically improved passing to the PS technique. Of course, PS density and coherence level in a differential interferogram are strictly related quantities. Information carried by many PS can be completely lost using the

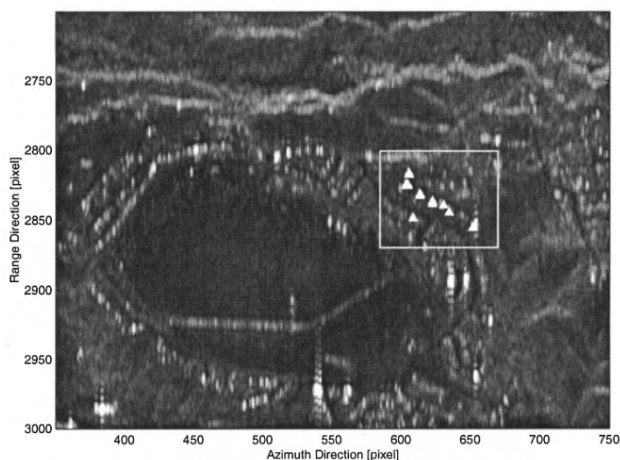


Fig. 14. Multi-image reflectivity map of the area represented in Figs. 12 and 13. The white “up-triangles” identify a group of similar targets showing a very small dispersion of their relative elevations.

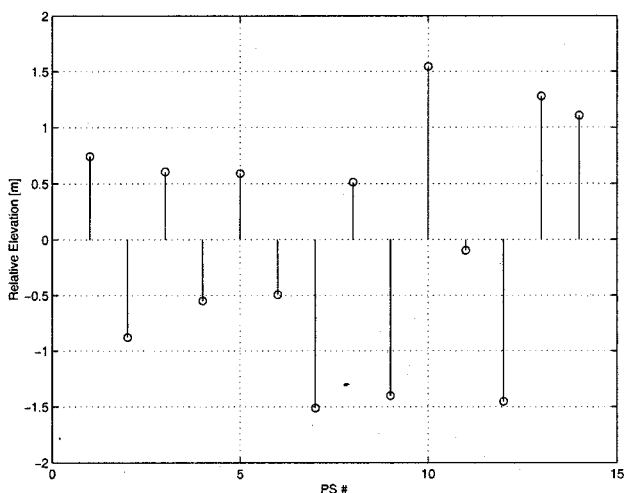


Fig. 15. Relative elevation (with respect to their mean value) of the pixels highlighted in Fig. 14. The standard deviation is 1 m.

single interferogram approach. Interferograms stacking [24] can strongly improve the reliability of the results (again using more interferograms of the same area), but slope estimation techniques can give rise to severe errors when the SNR ratio is too low. On the contrary, no spatial smoothing is carried out by the PS approach and single coherent pixels can be identified and successfully exploited.

*E. PS Density and DEM Optimization*

In Fig. 11, the relation between the LPR values of the PSs and their areal density is shown. Statistics was computed considering areas where the constant velocity model was valid. It appears that in urban areas, we have very many PSs, and this could be a very important indicator of the possibilities of the PS technique to estimate preseismic motions.

In Figs. 12 and 13, we see the effect of the DEM refinement carried out by the algorithm (with a significant magnification of the vertical dimension). This area corresponds to the bottom-left part of Fig. 1. Of course, elevation values can be optimized only

where PS are available. In Fig. 14, a group of similar targets is highlighted and in Fig. 15, we show the distribution of their relative elevations with respect to their mean value. If we hypothesize that buildings in this area have similar heights, the dispersion of the distribution tells us about the precision of the elevation estimate. If we suppose that phase residues due to decorrelation noise, residual (nonlinear) motion, and residual atmospheric components have rms value of less than 1 rad, we expect the elevations, estimated using the periodogram technique, to have a dispersion of about 0.5 m [1]. This simple analysis confirms at least the order of magnitude of the precision of the estimate.

It is important to point out that though the phase signature of a building often depends on multipath scattering and does not necessarily reflect the height of the building, it is unlikely that this is true for the case under study. In fact, if the scattering mechanism were dominated by multibounce effects, we would not have such a low phase dispersion notwithstanding the high variation of the baseline values. As shown in [1], the dimensions of a PS are significantly smaller than the resolution cell. Thus, it is only slightly affected by geometric decorrelation.

V. CONCLUSIONS

We have presented another application of the technique of PSs for differential interferometry studies. The usefulness of the gigantic data set of the ERS 1/2 images and the possibility of going back to 1992 have been stressed again. Another remark is that the irregularities of the acquisitions (in this case, due to the competition of the geodetical phase of ERS-1) have negative effects. This shows that a sizeable part of the operation time of a SAR system should be devoted to acquiring data systematically to avoid acquisition holes that weaken the entire data series.

ACKNOWLEDGMENT

The authors would like to thank Dr. G. Rigamonti and Dr. R. Locatelli for their support in data processing and N. Bienati for helpful discussions on phase unwrapping on a sparse grid. The continuous support of ESA and namely of Dr. L. Marelli, Dr. M. Doherty and Dr. B. Rosich, has been extremely useful. The authors also wish to thank the reviewers, who gave helpful suggestions.

REFERENCES

- [1] A. Ferretti, C. Prati, and F. Rocca, “Permanent scatterers in SAR interferometry,” *IEEE Trans. Geosci. Remote Sensing*, vol. 38, pp. 2202–2212, Sept. 2000.
- [2] —, “Permanent scatterers in SAR interferometry,” in *Proc. Int. Geosci. Remote Sensing Symp.*, Hamburg, Germany, June 28–July 2 1999, pp. 1528–1530.
- [3] —, “Multibaseline InSAR DEM reconstruction: The wavelet approach,” *IEEE Trans. Geosci. Remote Sensing*, vol. 37, pp. 705–715, Mar. 1999.
- [4] A. Ferretti, C. Prati, F. Rocca, and A. Monti Guarnieri, “Multi-baseline SAR interferometry for automatic DEM reconstruction,” in *Proc. 3rd ERS Symp.*, Florence, Italy, 1997, <http://florence97.ers-symposium.org/>.
- [5] S. Williams, Y. Bock, and P. Pang, “Integrated satellite interferometry: Tropospheric noise, GPS estimates and implications for interferometric synthetic aperture radar products,” *J. Geophys. Res.*, vol. 103, no. B11, pp. 27 051–27 067, 1998.
- [6] R. Hanssen, *Atmospheric Heterogeneities in ERS Tandem SAR Interferometry*. Delft, The Netherlands: Delft Univ. Press, 1998.

- [7] H. A. Zebker and P. Rosen, "Atmospheric artifacts in interferometric synthetic aperture radar surface deformation and topographic maps," *J. Geophys. Res.: Solid Earth*, vol. 102, pp. 7547–7563, 1997.
- [8] R. Bamler and M. Van Der Kooij, private communication.
- [9] C. L. Carilli and M. A. Holdaway, "Tropospheric phase calibration in millimeter interferometry," *Radio Sci.*, vol. 23, pp. 713–720, 1988.
- [10] M. Costantini and P. Rosen, "A generalized phase unwrapping approach for sparse data," in *Proc. Int. Geosci. Remote Sensing Symp.*, Hamburg, Germany, June 28–July 2 1999, pp. 267–269.
- [11] M. Costantini, "A novel phase unwrapping method based on network programming," *IEEE Trans. Geosci. Remote Sensing*, vol. 36, pp. 813–821, May 1998.
- [12] M. Eineder and J. Holzner, "Phase unwrapping of low coherence differential interferograms," in *Proc. Int. Geosci. Remote Sensing Symp.*, Hamburg, Germany, June 28–July 2 1999, pp. 1727–1730.
- [13] D. Ghiglia and M. Pritt, *Two-Dimensional Phase Unwrapping: Theory, Algorithms and Software*. New York: Wiley, 1998.
- [14] U. Spagnolini, "2-D phase unwrapping and instantaneous frequency estimation," *IEEE Trans. Geosci. Remote Sensing*, vol. 33, pp. 579–589, May 1995.
- [15] R. Goldstein, H. Zebker, and C. Werner, "Satellite radar interferometry: Two-dimensional phase unwrapping," *Radio Sci.*, vol. 23, pp. 713–720, 1988.
- [16] S. L. Marple, *Digital Spectral Analysis with Applications*. Englewood Cliffs, NJ: Prentice-Hall, 1987.
- [17] D. Rife and R. Boorstyn, "Single-tone parameter estimation from discrete-time observations," *IEEE Trans. Inform. Theory*, vol. 20, pp. 591–598, Sept. 1974.
- [18] S. Haykin, *Adaptive Filter Theory*. NJ: Prentice-Hall, 1991.
- [19] H. Wackernagel, *Multivariate Geostatistics*. Berlin, Germany: Springer-Verlag, 1998.
- [20] G. Gambolati, G. Ricceri, W. Bertoni, G. Brighenti, and E. Vuillermin, "Mathematical simulation of the subsidence of Ravenna," *Water Resource Res.*, vol. 27, no. 11, pp. 2899–2918, 1991.
- [21] G. Christakos and P. Bogaert, "Spatiotemporal analysis of spring water ion processes derived from measurements at the Dyle Basin in Belgium," *IEEE Trans. Geosci. Remote Sensing*, vol. 34, pp. 626–642, May 1996.
- [22] G. Peltzer. Monitoring of ground subsidence. [Online] Available <http://www.esrin.esa.it/esrin/eos/mon2.html>.
- [23] R. Scharroo, P. Visser, and G. J. Mets, "Precise orbit determination and gravity field improvement for the ERS satellites," *J. Geophys. Res.*, vol. 103, no. C4, pp. 8113–8127, 1998.
- [24] D. T. Sandwell and E. J. Price, "Phase gradient approach to stacking interferograms," *J. Geophys. Res.*, vol. 103, pp. 30 183–30 204, 1998.
- [25] S. Usai and R. Klees, "On the feasibility of long time scale INSAR," in *Proc. Int. Geosci. Remote Sensing Symp.*, Seattle, WA, July 6–10, 1998, pp. 2448–2450.
- [26] POLIMI SAR Group Web Page, Subsidence monitoring of Pomona, CA, by means of the PS Technique. [Online] Available <http://www-dsp.elet.polimi.it/andrea/www/sar/index.html>.



**Alessandro Ferretti** was born in Milano, Italy, on January 27, 1968. He received the "Laurea" and Ph.D. degrees, both in electrical engineering, from Politecnico di Milano (POLIMI), Milano, Italy, in 1993 and 1997, respectively, writing his dissertation on the use of multibaseline SAR interferograms for more reliable phase unwrapping algorithms. He received the "Master" degree in information technology from CEFRIEL (Politecnico—private firms consortium), Milano, Italy, in 1993.

In May 1994, he joined the POLIMI SAR Group, working with Prof. F. Rocca and Prof. C. Prati on SAR interferometry and digital elevation model reconstruction. He visited the Department of Geometric Engineering (formerly Photogrammetry and Surveying), University College, London, U.K., during the Summer of 1996. He is presently Managing Director and Co-Founder of Tele-Rilevamento Europa (TRE), a POLIMI commercial spinoff. His research interests concern digital signal processing and remote sensing.

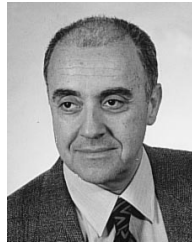


**Claudio Prati** was born in Milano, Italy, on March 20, 1958. He received the Laurea degree in electronic engineering in 1983 and the Ph.D. degree in 1987, both from the Politecnico di Milano.

In 1987, he joined the Centro Studi Telecomunicazioni Spaziali, National Research Council, Milano. He visited the Department of Geophysics, Stanford University, Stanford, CA, as a Visiting Scholar during the Autumn Quarter of 1987. Since 1991, he has been an Associated Professor of Systems for Remote Sensing, Politecnico di Milano.

He has been responsible for the interferometric experiments at the European Microwave Signature Laboratory (EMSL), Joint Research Center, Ispra, Italy. His main research interests concern digital signal processing in noise suppression, emission tomography, and synthetic aperture radar (SAR), where he has studied new focusing techniques and interferometrical applications of SAR data. He has written more than 50 papers on these topics.

Prof. Prati received the IEEE Geoscience and Remote Sensing Society 1989 Symposium Prize Paper award. He holds, with Prof. F. Rocca, U.S. Patent N 5 332 999 (July 26, 1994) on a "Process for generating Synthetic Aperture Radar Interferograms."



**Fabio Rocca** received the Dottore degree in ingegneria elettronica from the Politecnico di Milano, Milano, Italy, in 1962.

He is currently with the Department of Electronic Engineering, Politecnico di Milano, where he is Professor of digital signal processing. His research activities in seismics were dedicated to multi-channel filtering, interpolation of faulted surfaces, migration in the frequency domain, dip moveout processing, non-linear deconvolution, offset and shot continuation, and recently, using drill bit noise

for "while drilling" investigations. His nonseismic research activities have been dedicated to television bandwidth compression, where he introduced and analyzed the technique of motion compensation, in emission tomography and in synthetic aperture radar (SAR). He was President of the Osservatorio Geofisico Sperimentale, Trieste, Italy, from 1982 to 1983, where he is now Coordinator of the Scientific Council.

Prof. Rocca is a member of the Scientific Council of the Institut Français du Pétrole, Paris, France. He is Past President and Honorary Member of the European Association of Exploration Geophysicists and Honorary Member of the Society of Exploration Geophysicists. He was awarded the Honeywell International Award (HUSPI) for biomedical image processing applications in 1979, the Symposium Prize Paper Award at IGARSS '89, the 1990 Schlumberger Award of the EAGE, and the Italgas Award for Telecommunications in 1995.